# Protection Coordination System for a Converter Dominated Standalone DC Microgrid

Md Rifat Kaisar Rachi, Mehnaz Akhter Khan, and Iqbal Husain
FREEDM Systems Center
North Carolina State University
Raleigh, NC, USA
Email: {mrachi, makhan4, ihusain2}@ncsu.edu

***Abstract*—In this work, a reliable coordination system between fast protection devices and power electronic converters in a standalone DC microgrid is presented. The system is a standalone DC microgrid which is supplied by the distributed energy resources of an emulated wave energy converter and an energy storage unit. A system model that includes solid-state circuit breakers is developed in PLECS to analyze the steady-state operation as well as faulted conditions. Fault diagnosis and detection have been carried out in different segments of the system for both overcurrent and short-circuit faults. An effective protection coordination system is developed considering current limiting operation of power electronic converter during fault to ensure rapid fault isolation and continued power delivery to the healthy segments. The protection algorithm demonstrates reliable system operation and fault isolation during an event of overcurrent or short-circuit fault. Experimental results are presented to validate successful operation of the solid-state circuit breaker in a 380V DC system.**

***Keywords— DC microgrid; power electronic converter; fault; current limit; circuit breaker***

## I. Introduction

Proliferation of advanced power electronic converters with superior control and enhanced efficiency has made renewable resource integration cost-effective in both industrial and public sectors [1]. This facilitates reduced dependency on fossil fuel to cut down greenhouse gas emissions which is the most significant concern of this era. Also, leveraging local resources through standalone microgrid based distribution network to meet electric power requirement leads to building a more resilient community in the event of a climatic catastrophe. Although, majority of the implemented microgrids are AC in nature, DC microgrid has started to emerge as a suitable power distribution architecture in recent years because it can accommodate distributed energy resources directly without additional power conversion stages thus having higher system efficiency [2]. In addition, DC microgrids benefit from simplified control without having the complexities of an AC microgid such as phase synchronization, harmonics, and active and reactive power control [3]. This makes it highly suitable, specially for the increasing DC loads such as electronic equipment, electric vehicles and data centers.

Despite numerous benefits of DC distribution system with power electronic converter, wide scale adaptation of DC microgrid is still limited, since designing a suitable protection system for this kind of power network is much more challenging compounded by the fact that DC protection devices still need innovations and development [4]–[6]. The problem is multifold and each requires careful consideration. First, DC lacks zero crossing which makes current interruption and more importantly arc quenching followed by fault clearing much more challenging compared to an AC system [7]. To use mechanical circuit breakers similar to that of AC system, breakers have to be severely oversized for successful fault isolation. Recently, solid-state circuit breakers are developed to address this issue [8], [9]. They provide much faster isolation compared to their mechanical counterpart making them highly suitable for DC application. Also, the current rise rate is extremely high in a DC distribution system due to low system impedance [4]. Another major challenge is low overcurrent tolerance of the power electronic converters due to the limitations of the solid-state devices employed. Control systems for these converters are formulated considering this limitation and converters go into a current limiting mode during overloading to protect its components which results in output bus voltage collapse. While current magnitude based protection works well in legacy AC distribution system, this cannot be adopted directly for a converter dominated DC microgrid as it will lead to delayed breaker operation due to the limited fault current availability [10]. Coordinated operation between fast protection devices and converters considering converter behavior during fault is the key requirement to maximize continued power delivery to the healthy segments during fault.

The rest of the paper is organized as following: in Section II, a standalone DC microgrid with power electronic converter interfaced distributed energy resources is modeled with solid-state DC circuit breakers (SSDCCB) as protective elements. It is broken down to several zones for fault analysis. In section III, fault diagnosis is carried out in different zones for both overcurrent and short-circuit faults and protection coordination requirement is analyzed. Current limiting behaviour of converters is considered for proper SSDCCB operation during overload. However, breaker operation requirement during bolted fault is also specified. Finally in Section IV, experimental results are provided to demonstrate successful fault isolation with the adopted protection coordination while continuing converter operation for a 380V DC system.

978-1-7281-0395-2/19/$31.00 ©2019 IEEE

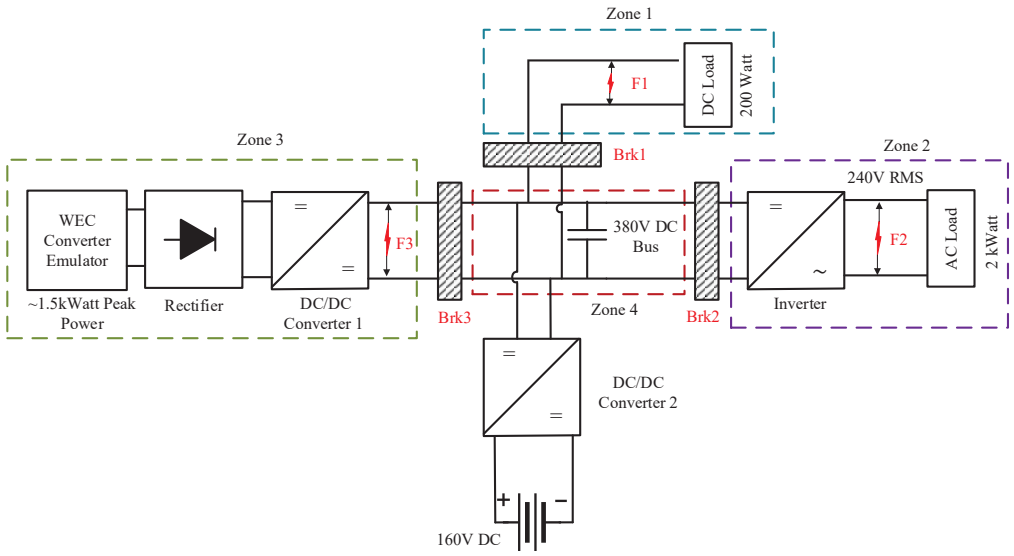


Fig. 1: Standalone coastal microgrid with WEC and its different fault diagnosis zones.

## II. Standalone DC Microgrid with Solid-State Circuit Breaker

A converter dominated standalone DC microgrid with a wave energy converter (WEC) as renewable resource, a storage unit and several fast protection devices is first simulated to analyze system behaviour during overload and short-circuit condition to develop the necessary protection coordination algorithm.

### *A. Standalone DC Microgrid*

Fig. 1 illustrates the overall system architecture of a standalone DC microgrid with WEC. Hydrokinetic resources such as the ocean wave has vast potential to provide clean energy due to its high power density [11]. Standalone DC microgrid with WEC can provide energy support to multiple applications like seawater desalination, subsea datacenter, and aquaculture. The WEC emulated here is considered to be of Wave Follower type in nature that produces torque proportional to wave speed [12]. Wave speed data is taken from EPRI survey report on mapping and assessment of the US ocean wave energy resources [11]. Torque proportional to wave speed is then applied to drive a permanent magnet synchronous generator to get oscillatory electrical power output. The output from WEC is coupled to the whole system through a rectifier and DC/DC converter 1. DC/DC converter 2 is a bi-directional converter that interfaces the storage unit to the microgrid and it is responsible to maintain the 380V DC bus. The load is modeled for a desalination plant, which makes this standalone coastal microgrid viable for deployment near remote islands. Majority of load of a desalination plant is inverter driven motor loads accounting for multiple pumps present in such system [13]. ∼10% of load is DC powering its auxiliary units. A scaled down system is shown in Fig. 1. It has 2kW of inverter connected load and 200W DC load.

Fig. 2 shows the wave speed profile and respective WEC generated power. The peak output power from the WEC is ∼1.5kW for this 20s simulation window. The average current outputs from the WEC and the storage unit are shown in Fig. 3. Dips can be seen in battery current profile corresponding to current output from the WEC unit implying that the WEC is providing part of the load. Negative current on storage unit implies excess available power from the WEC that goes into charging.

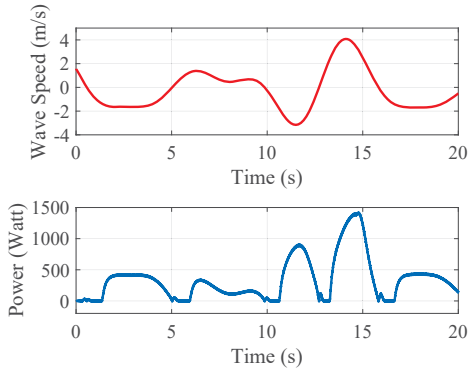


Fig. 2: Wave speed and power generated from single WEC.

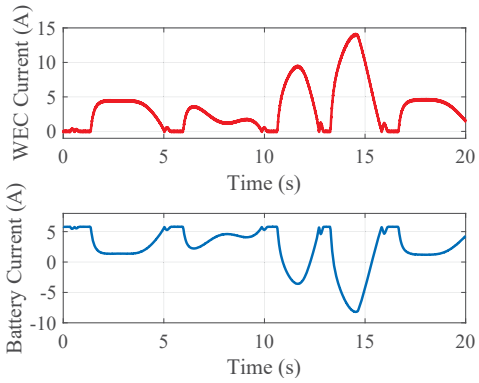


Fig. 3: Current output from WEC and storage unit.

Fig. 4 shows the control loop adopted in the storage interfacing single leg bi-directional converter. It saturates the internal current reference to a maximum value forcing the converter to operate in the current limiting mode during overload to ensure safe operation of solid-state switches. However, this lowers the bus voltage from 380V and limited current output leads to unreliable circuit breaker operation if only current magnitude based fault detection is adopted.

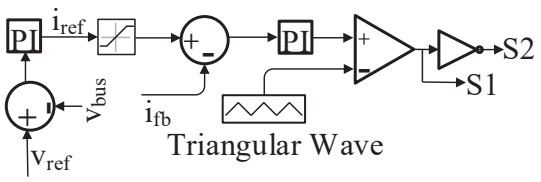


Fig. 4: Dual loop current limiting converter control.

Figs. 5 and 6 illustrate the converter output behavior of converter current and DC Bus voltage for 250% and 300% overload, respectively. The overload initiates at $t$ = 0.1s and is removed at $t$ = 0.3s. The current gets limited and output voltage falls. The converter follows a soft-start routine to suppress voltage spike after overload removal.

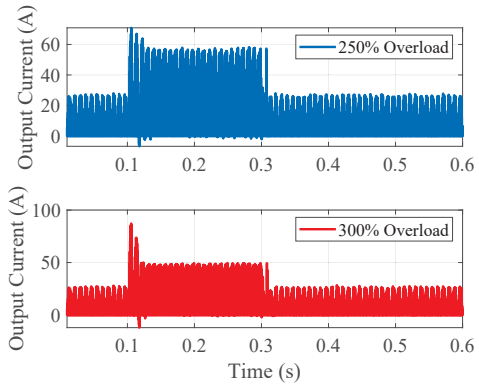


Fig. 5: Converter operating in current limiting mode.

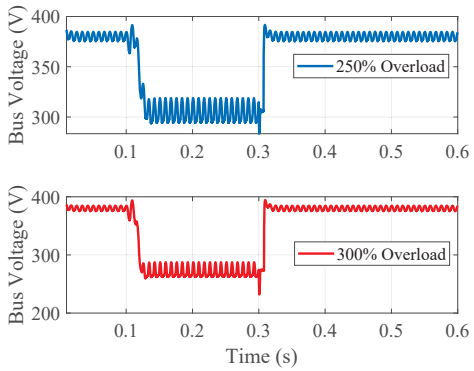


Fig. 6: Bus voltage collapse due to overload.

### B. Rule Base for Protection Coordination

Current limiting behaviour of the power electronic converter described in the previous segment needs careful consideration while developing protection coordination algorithm. This applies to any converter dominated microgrid network in general, irrespective of the nature of distributed energy resources as post-fault dynamics only depends on the converter controller design and the solid-state device absolute rating. The rule base followed for coordination among breakers and converters are as following-

- If fault current magnitude is lower than converter current limit, then inverse time current curve is sufficient for coordinated operation of breakers while converters continue to operate without de-energizing.
- If converter goes into current limiting mode, then voltage magnitude based coordination is required to ensure fault isolation before converter shutdown.
- During bolted fault/short-circuit, instantaneous tripping of SSDCCB is required which is initiated by device gate driver circuit.

The procedures to adopt these generalized rules in a solid-state circuit breaker during overcurrent/short-circuit fault in a standalone DC microgrid network are presented in the following section.

### C. Solid-State DC Circuit Breaker

Fig. 7 shows the schematic for the solid-state circuit breaker used in this work. The circuit breaker allows bi-directional power flow which is a major requirement in DER integration in a DC microgrid. It employs two current sensors and a voltage sensor. All the sensors are equipped with low pass RC (R=100 Ω, C= 33 pF) filters to reduce unwanted noises in the measurements. Two current sensors allow to identify a ground fault if this breaker is adopted in a grounded system. The voltage sensor is utilized to measure bus voltage collapse when converter operates in the current limiting mode during overload and adopt a voltage based protection coordination method so that it isolates faults before the converter shuts down de-energizing the whole system.

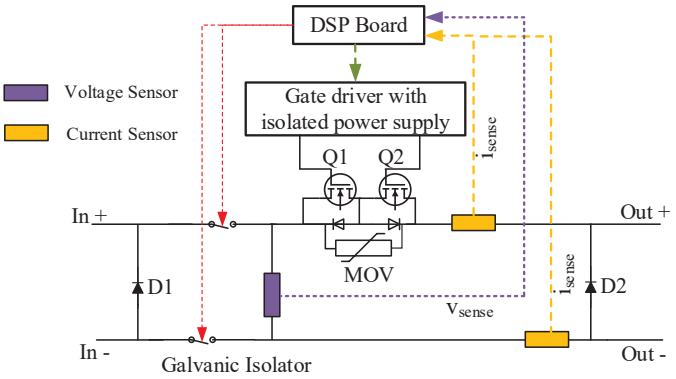


Fig. 7: Solid-state DC circuit breaker schematic.

## III. Fault Analysis and Protection Coordination

The standalone DC microgrid is segmented into four zones for fault analysis as shown in Fig. 1. Each zone either contains load or power source. Three solid-state circuit breakers (Brk1,

Brk2, Brk3) separate these zones. Two types of fault are considered for analysis: i) Overcurrent and ii) Short-circuit. Fault locations are shown in Fig 1 (F1, F2 and F3). Both faults are applied to zone 1 and zone 2. For zone 3, only short-circuit is considered since there is no load in this zone. In addition, no breaker is placed in front of converter 2, as this unit will shut down itself if there is a fault in zone 4.

### A. Overloading in Zone 1 (DC Branch)

Nominal DC load in zone 1 is 200W. An inverse time current characteristic (ITCC) trip routine is executed in Brk1 to isolate this zone during overload. It has the following mathematical formulation:

$$t_d = \frac{C}{(\frac{I}{I_{PU}})^2 - 1} \tag{1}$$

where $t_d$ represents the time delay before breaker operation, $I$ is the steady-state overcurrent, $I_p$ is breaker pickup current threshold, and $C$ is a constant. The pick up current and constant is chosen based on system specification. Here, $C$ is chosen to be 0.16 for breaker 1. $I_p$ is derived from the nominal load specification. Necessary time delay is generated based on fault current magnitude before the breaker isolates the fault. Additional 200W and 300W resistive DC load are applied at $t_i$=0.1s, respectively as overloads. The breaker detects the overload and isolates this branch following a delay calculated from Eq. 1 as shown in Fig. 8. The breaker operates faster ($t_f$ = 0.15s and $t_f$ =0.13s, respectively) for higher overloading condition. As the DC load is very low compared to the total load, the bus voltage does not collapse during overloading in zone 1.

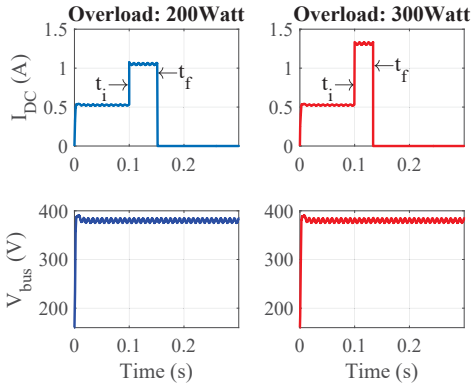


Fig. 8: Overload in zone 1 and subsequent breaker (Brk1) operation.

### B. Overloading in Zone 2 (AC Branch)

Nominal AC load in zone 2 is 2kW as shown in Fig. 1. Additional 2kW and 3kW resistive loads are applied at $t_i$=0.1s for simulating overload. It forces converter 2 to operate in current limiting mode collapsing the bus voltage. The output current goes to a high value initially but gets limited as shown in Fig. 9. For reliable operation, a voltage-based protection logic is provided on top of an ITCC routine as shown in Eq. 1 for Brk2. Similar to ITCC routine, delay time before fault isolation is calculated based on terminal voltage.

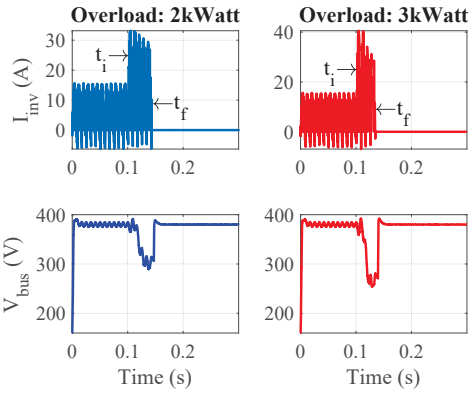


Fig. 9: Overload in zone 2 and subsequent breaker (Brk2) operation.

The voltage based protection coordination is developed using the voltage tolerance curve developed by EPRI for 380V DC system [14], shown in Fig. 10. Average DC bus voltage is tracked and necessary time delay is generated utilizing this curve before breaker 2 operates.

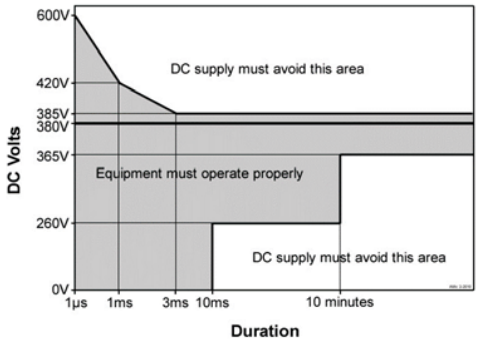


Fig. 10: Voltage tolerance curve for 380V DC system by EPRI.

Converter 2 provides back-up protection if breaker Brk2 fails to operate during overload in zone 2. Operation coordination is time graded between breaker 2 and converter 2 so that the converter only shuts down if the breaker fails. However, the coordinated operation of the breaker and converter is arranged such that system operating condition always falls within the shaded region shown in Fig. 10.

### C. Bolted Fault in Zone 1 and Zone 2

Bolted short circuits in zone 1 and zone 2 are investigated next for protection coordination. The objective is to ensure continued power delivery to the unaffected segments during short-circuit in one zone. Bolted fault results in rapid current rise (limited by system inductance only) which requires instant isolation. Commercial power device gate drivers are equipped with 'Desat' protection, which utilizes the device themselves as current sensing unit and shuts them down if the device current is higher than the maximum allowable current, which happens during bolted fault [15]. In simulation, 'Desat'

protection behavior of a commercial solid-state device gate driver is mimicked for driving solid-state switches present in the breakers and converters. It shuts down the switches below 1ms upon 'Desat' detection. The time delayed methods (current/voltage based) for overload protection require several hundred microseconds to act even for sensors with minimum delay, high sampling rate and fast microprocessors. 'Desat' protection from gate driver acts much faster than that during short-circuit providing instantaneous isolation.

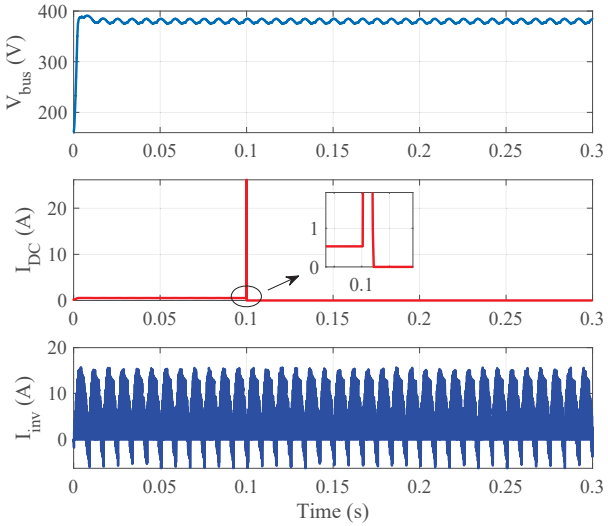


Fig. 11: Bolted fault in zone 1 and subsequent breaker (Brk1) operation.

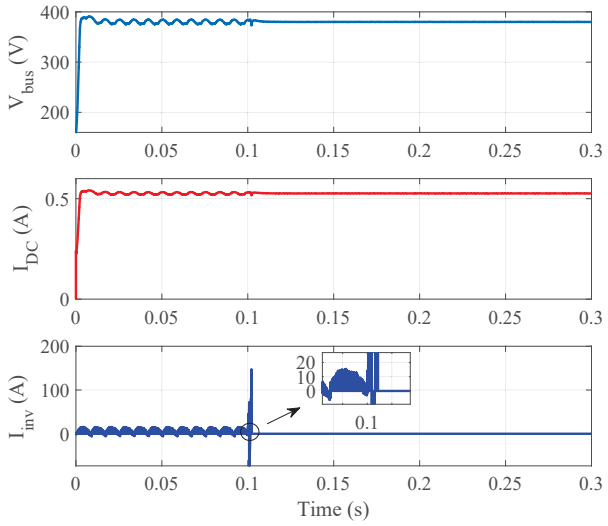


Fig. 12: Bolted fault in zone 2 and subsequent breaker (Brk2) operation.

For loads shown in Fig. 1, peak currents in zone 1 and zone 2 are 0.53Amp and 15Amp, respectively. Both for breaker 1 and 2, the Desat trip point is set at three times the nominal current value. For currents below this, regular overcurrent trip routine is followed. Figs. 11 and 12 illustrate the effect of bolted fault in zone 1 and 2 as well as subsequent breaker operation. Line inductance (assumed to be 100$\mu$H) in those zones limit short-circuit current peak. The bus voltage remains at its nominal value after fault isolation for both cases.

### D. Bolted Fault in Zone 3

For bolted fault in zone 3, it is assumed that this zone has significantly lower line inductance compared to zone 1 and 2 to study bus voltage behavior under this circumstance. Breaker 3 is also simulated with 'Desat' protection. For very low inductance on this segment, the bus voltage collapses rapidly as shown in Fig. 13. However, Brk3 acts instantaneously isolating the fault and bringing the bus to its nominal value. Both zone 1 and zone 2 continues to receive power during this.

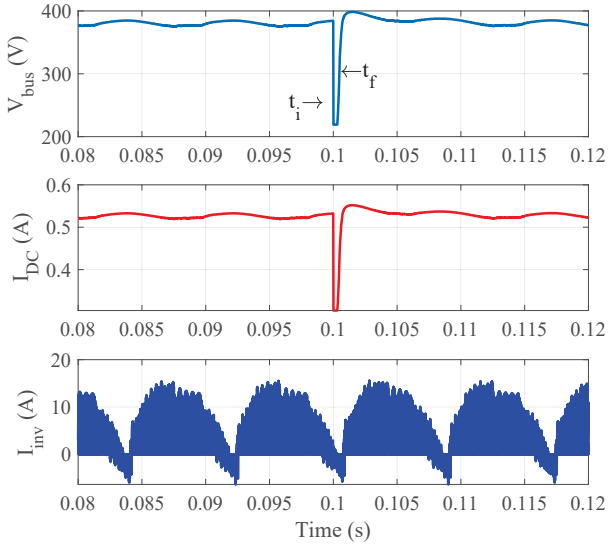


Fig. 13: Bolted fault in zone 3 and subsequent breaker (Brk3) operation.

Converter 2 provides back-up protection if any breaker fails to operate during overcurrent or bolted fault in their own protection zone. The solid-state switches in the converter have their own 'Desat' protection from gate driver. The devices in converter 2 are set to have higher current capability than those in breakers. This higher instantaneous trip threshold ensures its continued operation during faults in other three zones. This guarantees coordinated operation of converters and breakers.

### E. Breaker Control Flowchart

Fig. 14 illustrates the detailed flowchart adopted in the implemented solid-state circuit breaker leveraging both voltage and current information. Here, $I_{INST}$ denotes instantaneous trip current; $I_{PU}$ represents pick up current for ITCC trip curve; $V_{THRS}$ is the threshold voltage to activate voltage based protection; $t_i$ and $t_v$ are time delay generated from ITCC trip curve and voltage tolerance curves, respectively. If the converter goes into a current limiting mode, then the breaker operates after the minimum of $t_i$ and $t_v$ has passed thus ensuring fast and reliable fault isolation.

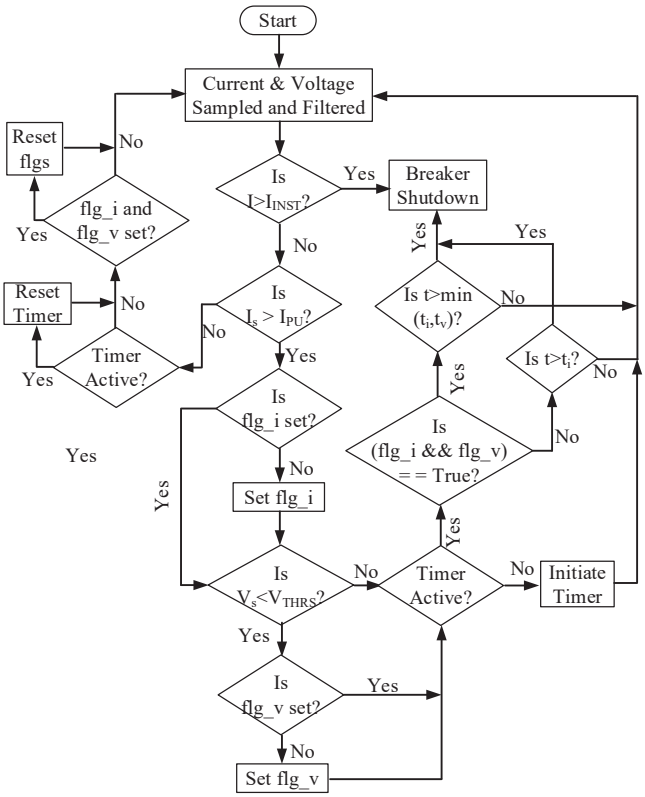


Fig. 14: Solid-state circuit breaker operation algorithm.

## IV. Experimental Results

Successful operation of the circuit breaker both during regular overcurrent and bus voltage collapsing mode are validated experimentally. A high bandwidth DC voltage source is utilized to emulate the bus controlling converter.

Fig. 15 shows the solid-state DC circuit breaker with DSP control board where the proposed dual current-voltage information based fault detection and isolation algorithm is implemented. The implemented system can block up to 900V and break up to 36A. It is used to emulate both Brk1 and Brk2.

The inverse time current characteristic curve shown in Fig. 16 is implemented in the controller to isolate fault after a fixed time delay based on the overload magnitude. This also shows a ”Instantaneous trip” region where the breaker trips instantly irrespective of the fault current magnitude.

### A. Converter Operating in Normal Mode

For this segment, the converter is configured such that it can supply the necessary fault current and the performance of the breaker control is evaluated.

Fig. 17 shows the breaker operation utilizing the ITCC curve shown in Fig. 16. During nominal condition, 0.55Amp flows into the load from a 380V DC bus. When it is overloaded to twice its nominal value, necessary delay ($\approx$ 30ms) is calculated from the ITCC curve and then the breaker trips to isolate the fault. As the overload current is well within converter

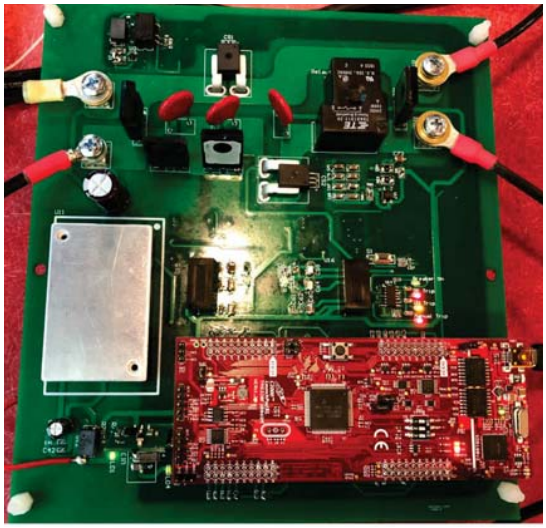

Fig. 15: Solid-state DC circuit breaker.

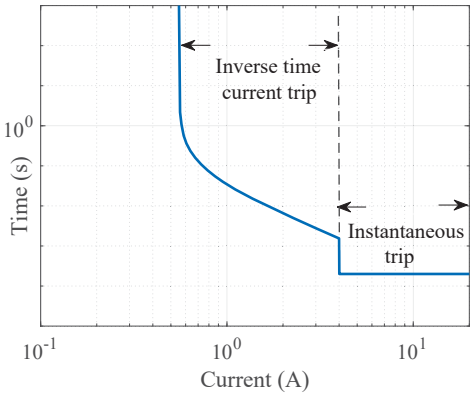


Fig. 16: Breaker trip curve.

current supplying capability, the bus voltage is maintained at 380V.

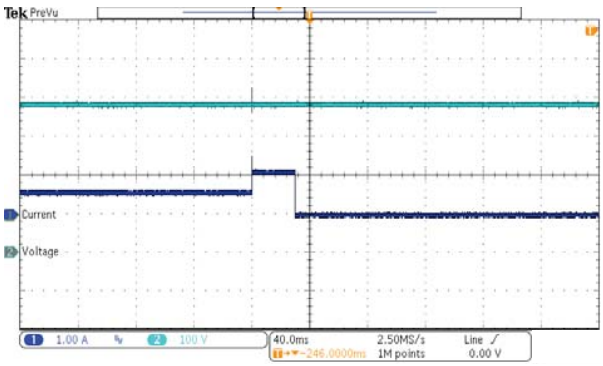


Fig. 17: Circuit breaker operation during overload using ITCC (Current: 1A/div; Voltage: 100V/div; Time: 40ms/div).

Fig. 18 shows the operation of the breaker during bolted fault. The fault current jumps to $\sim$5.63Amp which can be considered to be bolted fault for a 0.55Amp nominal current system. The breaker operates in the “Instantaneous trip” zone in this case isolating the fault within 0.2ms

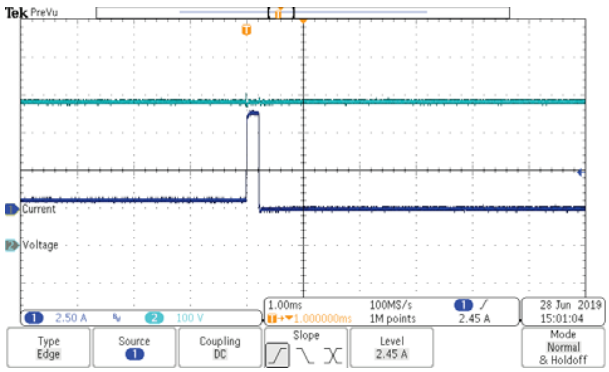


Fig. 18: Instantaneous fault isolation during bolted fault with low nominal current (Current: 2.5A/div; Voltage: 100V/div; Time: 1ms/div).

Both Figs. 17 and 18 illustrate operation of Brk1 that protects the low power DC load branch as shown in Fig. 1.

Fig. 19 illustrates another bolted fault scenario but with high nominal load (∼8.63Amp). Here, the breaker isolates ∼17.2Amp within 0.4ms isolating the system fault. This represents Brk2 operation.

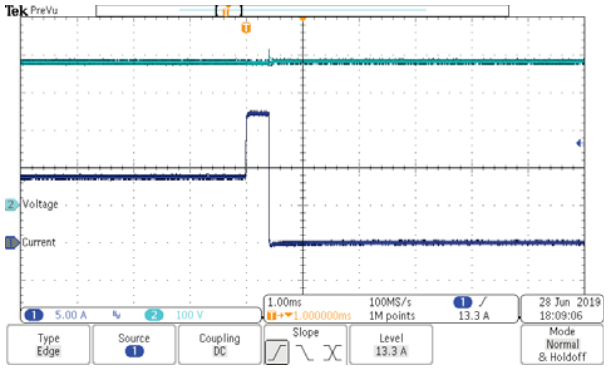


Fig. 19: Instantaneous fault isolation during bolted fault with high nominal current (Current: 5A/div; Voltage: 100V/div; Time: 1ms/div).

### *B. Converter Operating in Current Limiting Mode*

In this segment, the output voltage collapse of bus controlling converter is emulated by limiting the DC source's output current during fault and the breaker performance is evaluated.

Fig. 20 illustrates first instance of bus voltage collapse. The source is configured such that it can emulate a converter which can only supply up to 80% of the required fault current. This forces its output voltage to collapse to ∼325V from 380V. Voltage tolerance curve based protection segment is activated for this case and the breaker isolates the fault within 8ms. After the fault is cleared, the output voltage goes back to its nominal value. The magenta line denotes the breaker's fault identification and isolation time.

Fig. 21 shows the zoomed view for the scenario presented in Fig. 20. It clearly depicts that the breaker operates within the 8ms time interval.

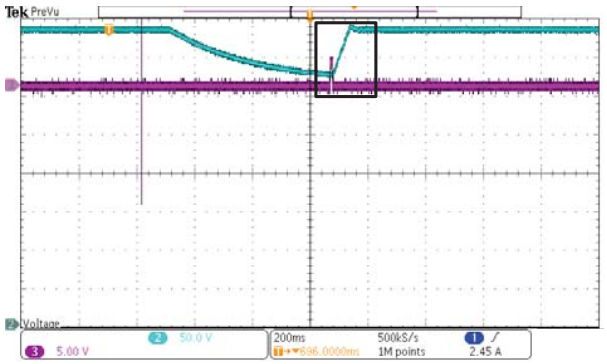


Fig. 20: Post-fault bus voltage collapse (to 325V) and its restoration after fault clearance (Voltage: 50V/div; Time: 200ms/div).

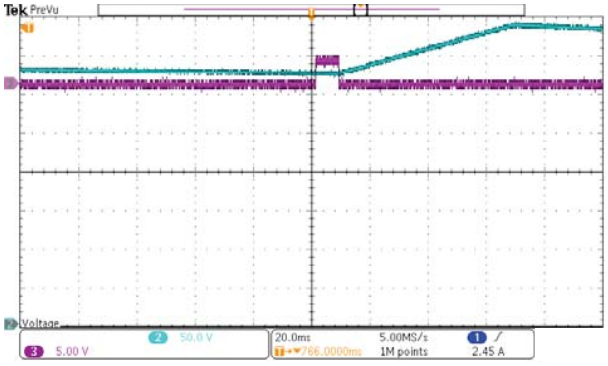


Fig. 21: Zoomed view of voltage collapsing to 325V and returning to nominal value after fault isolation (Voltage:50V/div; Time: 20ms/div).

Fig. 22 and Fig. 23 illustrate the second bus voltage collapse scenario and its zoomed view respectively. In this case the source is configured to supply 75% of the required fault current which results in lower bus voltage (∼308V). Again, the voltage tolerance curve based fault isolation procedure is executed (isolation time 5ms) and the bus voltage regains its nominal value.

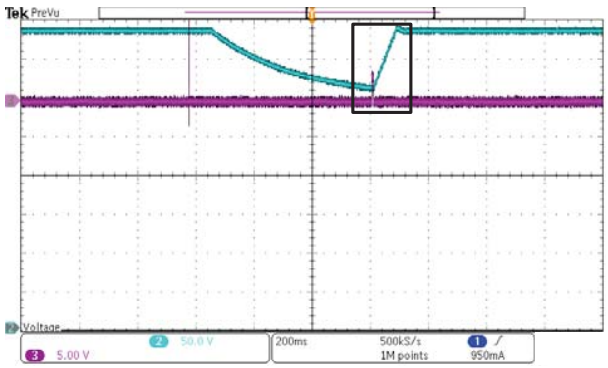


Fig. 22: Post-fault bus voltage collapse (to 308V) and its restoration after fault clearance (Voltage: 50V/div; Time: 200ms/div).

For both of the cases, the breaker operation ensures that the

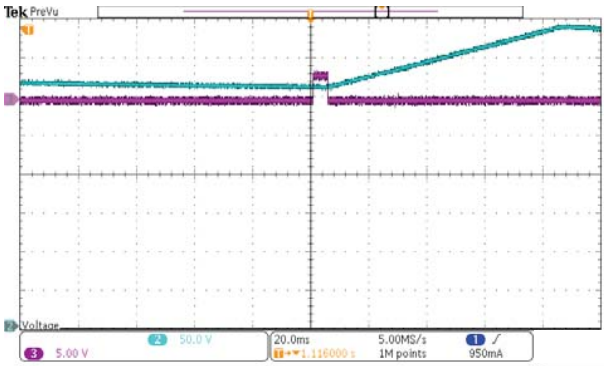


Fig. 23: Zoomed view of voltage collapsing to 308V and returning to nominal value after fault isolation (Voltage: 50V/div; Time: 20ms/div).

converter operation remains within the grey region shown in Fig. 10 which is the valid operational zone for the converter.

## V. Conclusion

Protection coordination system for a standalone DC microgrid is developed and experimentally demonstrated to validate reliable circuit breaker operation during both overcurrent and short-circuit faults. Current limiting behaviour of power electronic converter is utilized on top of regular current magnitude based approach for successful fault detection and consequent zone isolation through solid-state circuit breakers during overcurrent faults. Gate drivers' capability is leveraged for instantaneous breaker tripping during short-circuit. This adopted protection coordination ensures continued power delivery to healthy segments of the system during an event of fault. This method of protection coordination is independent of the nature of distributed energy resources integrated into DC microgrid through power electronic converter and can be extended to wide range of DC microgrid application.

## Acknowledgement

The authors would like to acknowledge the support of the University of North Carolina Coastal Studies Institute for carrying out this research work.

## References

[1] S. Mirsaeidi, X. Dong, S. Shi, and D. Tzelepis, "Challenges, advances and future directions in protection of hybrid ac/dc microgrids," *IET Renewable Power Generation*, vol. 11, no. 12, pp. 1495–1502, 2017.

[2] T. Dragievi, X. Lu, J. C. Vasquez, and J. M. Guerrero, "Dc microgridspart ii: A review of power architectures, applications, and standardization issues," *IEEE Transactions on Power Electronics*, vol. 31, no. 5, pp. 3528–3549, May 2016.

[3] D. Kumar, F. Zare, and A. Ghosh, "Dc microgrid technology: System architectures, ac grid interfaces, grounding schemes, power quality, communication networks, applications, and standardizations aspects," *IEEE Access*, vol. 5, pp. 12 230–12 256, 2017.

[4] N. Bayati, A. Hajizadeh, and M. Soltani, "Protection in dc microgrids: a comparative review," *IET Smart Grid*, vol. 1, no. 3, pp. 66–75, 2018.

[5] D. Salomonsson, L. Soder, and A. Sannino, "Protection of low-voltage dc microgrids," *IEEE Transactions on Power Delivery*, vol. 24, no. 3, pp. 1045–1053, July 2009.

[6] J. Park and J. Candelaria, "Fault detection and isolation in low-voltage dc-bus microgrid system," *IEEE Transactions on Power Delivery*, vol. 28, no. 2, pp. 779–787, April 2013.

[7] R. M. Cuzner and G. Venkataramanan, "The status of dc micro-grid protection," in *2008 IEEE Industry Applications Society Annual Meeting*, Oct 2008, pp. 1–8.

[8] Z. J. Shen, A. M. Roshandeh, Z. Miao, and G. Sabui, "Ultrafast autonomous solid state circuit breakers for shipboard dc power distribution," in *2015 IEEE Electric Ship Technologies Symposium (ESTS)*, June 2015, pp. 299–305.

[9] Z. J. Shen, G. Sabui, Z. Miao, and Z. Shuai, "Wide-bandgap solid-state circuit breakers for dc power systems: Device and circuit considerations," *IEEE Transactions on Electron Devices*, vol. 62, no. 2, pp. 294–300, Feb 2015.

[10] H. J. Laaksonen, "Protection principles for future microgrids," *IEEE Transactions on Power Electronics*, vol. 25, no. 12, pp. 2910–2918, Dec 2010.

[11] *"Mapping and Assessment of the United States Ocean Wave Energy"*. Electric Power Research institute (EPRI): Palo Alto, CA, USA, 2011.

[12] J. Prudell, M. Stoddard, E. Amon, T. K. A. Brekken, and A. von Jouanne, "A permanent-magnet tubular linear generator for ocean wave energy conversion," *IEEE Transactions on Industry Applications*, vol. 46, no. 6, pp. 2392–2400, Nov 2010.

[13] T. Yoshihara, A. Yokoyama, M. Imanaka, Y. Onda, J. Baba, Y. Kuniba, N. Higa, and S. Asato, "A new method for securing regulating capacity for load frequency control using seawater desalination plant in small island power system," in *2010 International Conference on Power System Technology*, Oct 2010, pp. 1–6.

[14] D. Symanski and C. Watkins, "380vdc data center at duke energy," Nov 2010.

[15] T. Instruments, "Iso5852s high-cmti 2.5-a and 5-a reinforced isolated igbt, mosfet gate driver with split outputs and active protection features," Jan 2017.